Capsid-like particles decorated with the SARS2-CoV-2 receptor-binding domain elicit strong virus neutralization activity

Cyrielle Fougeoux
AdaptVac https://orcid.org/0000-0002-7566-8377
Louise Goksøyr
University of Copenhagen
Manja Idorn
Aarhus University https://orcid.org/0000-0002-6769-9165
Vladislav Soroka
ExpreS2ion Biotechnologies (Denmark)
Sebenzile K. Myeni
Department of Medical Microbiology, Leiden University Medical Center
Robert Dagil
University of Copenhagen, Denmark https://orcid.org/0000-0002-5594-0716
Christoph M. Janitzek
University of Copenhagen
Teit Søgaard
ExpreS2ion Biotechnologies (Denmark)
Kara-Lee Aves
University of Copenhagen
Emma W. Horsted
University of Copenhagen
Sayit Mahmut Erdoğan
University of Copenhagen https://orcid.org/0000-0001-7120-1609
Tobias Gustavsson
Centre for Medical Parasitology at Department of Immunology and Microbiology, University of Copenhagen and Department of Infectious Diseases, Copenhagen University Hospital
Jerzy Dorosz
Expres2ion biotechnologies
Stine Clemmensen
ExpreS2ion Biotechnologies
Laurits Larsen
University of Copenhagen https://orcid.org/0000-0003-3891-3414

Susan Thrane
AdaptVac
Elena E. Vidal-Calvo
VAR2pharmaceuticals https://orcid.org/0000-0001-9655-2106
Paul Khalifé
University of Copenhagen https://orcid.org/0000-0001-6160-4674
Thomas M. Hulen
University of Copenhagen https://orcid.org/0000-0003-2475-6526
Swati Choudhary
Centre for Medical Parasitology at Department of Immunology and Microbiology, University of Copenhagen and Department of Infectious Diseases, Copenhagen University Hospital
Michael Theisen
Department of Congenital Diseases, Statens Serum Institut & Centre for Medical Parasitology at Department of International Health, Immunology and Microbiology, University of Copenhagen
Susheel Singh
Copenhagen University, Statens Serum Institute
Asier Garcia-Senosiain
University of Copenhagen
Linda Van Oosten
Department of Plant Sciences, Laboratory of Virology
Gorben Pijlman
Wageningen University https://orcid.org/0000-0001-9301-0408
Bettina Hierzberger
Expres2ion biotechnologies
Tanja Domeyer
Expres2ion biotechnologies https://orcid.org/0000-0002-3908-9546
Blanka W. Nalewajek
Expres2ion biotechnologies
Anette Strøbæk
Expres2ion biotechnologies
Magdalena Skrzypczak
Expres2ion biotechnologies https://orcid.org/0000-0001-6059-5059
Laura F. Andersson
Expres2ion biotechnologies
Tim Dalebout
Leiden University Medical Center
Kasper Iversen
Department of Cardiology, Herlev University Hospital, Herlev
Lene H. Harritshøj

Department of Clinical Immunology, Copenhagen University Hospital
Benjamin Mordmüller
University of Tübingen https://orcid.org/0000-0001-9101-2768
Henrik Ullum
Copenhagen University Hospital, Rigshospitalet
Line Reinert
Aarhus University https://orcid.org/0000-0002-8317-0886
Willem Adriaan de Jongh
AdaptVac
Marjolein Kikkert
Leiden University Medical Center
Soren Paludan
Aarhus University https://orcid.org/0000-0001-9180-4060
Thor Theander
University of Copenhagen
Morten Nielsen (✉ mortenn@sund.ku.dk)
Centre for Medical Parasitology at Department of Immunology and Microbiology, University of Copenhagen and Department of Infectious Diseases, Copenhagen University Hospital
Ali Salanti
University of Copenhagen and Department of Infectious Diseases, Copenhagen University Hospital
Adam Sander (✉ asander@sund.ku.dk)
University of Copenhagen

Article

Keywords: SARS-CoV-2, capsid-like particle, CLP, RBD-CLP vaccines, virus neutralization

Posted Date: July 28th, 2020

DOI: https://doi.org/10.21203/rs.3.rs-45062/v1

Version of Record: A version of this preprint was published at Nature Communications on January 12th, 2021. See the published version at https://doi.org/10.1038/s41467-020-20251-8.

Title

Capsid-like particles decorated with the SARS2-CoV-2 receptor-binding domain elicit strong virus neutralization activity

Cyrielle Fougeroux[1*], Louise Goksøyr[1,2*], Manja Idorn[3], Vladislav Soroka[4], Sebenzile K. Myeni[5], Robert Dagil[2,6], Christoph M. Janitzek[2], Max Søgaard[4], Kara-Lee Aves[2], Emma W. Horsted[2], Sayit Mahmut Erdoğan[2,7], Tobias Gustavsson[2,6], Jerzy Dorosz[4], Stine Clemmensen[4], Laurits Fredsgaard[2], Susan Thrane[1], Elena E. Vidal-Calvo[6], Paul Khalifé[2], Thomas M. Hulen[2], Swati Choudhary[2,6], Michael Theisen[2,8], Susheel Singh[2,8], Asier Garcia-Senosiain[2,8], Linda Van Oosten[9], Gorben Pijlman[9], Bettina Hierzberger[4], Tanja Domeyer[4], Blanka W. Nalewajek[4], Anette Strøbæk[4], Magdalena Skrzypczak[4], Laura F. Andersson[4], Tim J. Dalebout[5], Kasper Iversen[10], Lene H. Harritshøj[11], Benjamin Mordmüller[12,13], Henrik Ullum[11], Line S. Reinert[3], Willem Adriaan de Jongh[1,4], Marjolein Kikkert[5], Søren R. Paludan[3], Thor G. Theander[2], Morten A. Nielsen[2], Ali Salanti[2,6], Adam F. Sander[1,2]

[*] shared first authorship

[1] AdaptVac Aps, 2970 Hørsholm, Denmark

[2] Centre for Medical Parasitology at Department for Immunology and Microbiology, Faculty of Health and Medical Sciences, University of Copenhagen and Department of Infectious Disease, Copenhagen University Hospital, 2200 Copenhagen, Denmark

[3] Department of Biomedicine, Aarhus University, 8000 Aarhus, Denmark

[4] ExpreS[2]ion Biotechnologies Aps, 2970 Hørsholm, Denmark

[5] Department of Medical Microbiology, Leiden University Medical Center, ZA Leiden 2333, Netherlands

[6] VAR2pharmaceuticals, 2200 Copenhagen, Denmark

[7] Turkish Ministry of Agriculture and Forestry, 06800 Ankara, Turkey

[8] Department for Congenital Disorders, Statens Serum Institute, 2300 Copenhagen, Denmark

[9] Department of Plant Sciences, Laboratory of Virology, 6700AA Wageningen, Netherlands

[10] Department of Cardiology, Herlev Hospital, 2730 Herlev, Denmark

[11] Department of Clinical Immunology, Copenhagen University Hospital, 2100 Copenhagen, Denmark

[12] Universitätsklinikum Tübingen, Institut für Tropenmedizin, 72074 Tübingen, Germany

[13] Centre de Recherches Médicales de Lambaréné, BP 242 Lambaréné, Gabon

Corresponding authors:
Morten A. Nielsen (mortenn@sund.ku.dk) and Adam F. Sander (asander@sund.ku.dk)

Abstract

The rapid development of a SARS-CoV-2 vaccine is a global priority. Here, we developed two capsid-like particle (CLP)-based vaccines displaying the receptor-binding domain (RBD) of the SARS-CoV-2 spike protein. RBD antigens were displayed on AP205 CLPs through a novel split-protein Tag/Catcher ensuring unidirectional and high-density display of RBD. Both soluble recombinant RBD, and RBD displayed on CLPs bound the ACE2 receptor with nanomolar affinity. Mice were vaccinated with soluble RBD or CLP-displayed RBD, formulated in Squalene-Water-Emulsion. The RBD-CLP vaccines induced higher levels of serum anti-RBD antibodies, than the soluble RBD vaccines. Remarkably, one injection with our lead RBD-CLP vaccine in mice elicited virus neutralization antibody titers comparable to those found in patients which had recovered from Covid-19. Following booster vaccinations, the virus neutralization titers exceeded those measured after natural infection, at serum dilutions above 1:10.000. Thus, the RBD-CLP vaccine is highly promising candidates for preventing COVID-19 disease.

Introduction

Starting in December 2019, the Severe acute respiratory syndrome corona virus 2 (SARS-CoV-2) outbreak rapidly spread, and by March 2020, the World Health Organization (WHO) declared a public health emergency of international concern (PHEIC)[1]. SARS-CoV-2 belongs to the subfamily of *Coronavirinae* comprising at least seven members known to infect humans, including the highly pathogenic strains, SARS-CoV and Middle East respiratory syndrome corona virus (MERS-CoV)[2]. The symptoms of the disease (COVID-19) range from mild flu-like symptoms, including cough and fever, to life threatening complications. Both SARS-CoV and SARS-CoV-2 use highly glycosylated homotrimeric spike proteins to engage angiotensin-converting enzyme 2 (ACE2) on host cells to initiate cell entry[3–7]. The SARS-CoV spike proteins are known targets of protective immunity, eliciting both neutralizing antibodies and T-cell responses upon natural infection[8]. Consequently, the spike protein is a primary target for SARS-CoV-2 vaccine development, with emphasis on the receptor-binding domain (RBD), which appears to be the target for most neutralizing antibodies[9–15]. The urgent need of an effective SARS-CoV-2 vaccine, to contain the worldwide pandemic and prevent new viral outbreaks, has led to a global effort involving a wide range of vaccine technologies. These include genetic-based (mRNA and DNA) principles[16,17], replicating/non-replicating viral vectors (measles[18], adenovirus[19,20], baculovirus) recombinant proteins or peptides[21], virus-like particles (VLPs)/nanoparticles or inactivated and live-attenuated viral vaccines[22–24]. In fact, more than 120 SARS-CoV-2 candidate vaccines are currently registered by WHO, of which 21 are currently undergoing clinical testing[25]. We have developed a SARS-CoV-2 vaccine based on a platform similar to the well-characterized Tag/Catcher-AP205 derived

technology[26,27]. Accordingly, a split-protein Tag/catcher system[28,29,30] is used to conjugate and display the RBD of the SARS-CoV-2 spike protein on the protein surface of preassembled AP205 capsid-like particles (CLPs). CLPs are supramolecular structures assembled from multiple copies of a single viral coat protein, thus resembling the structure of the virus from which they are derived[31]. Importantly, CLPs are considered safe, as they do not contain any viral material and thus cannot infect or replicate[32]. Their resemblance with native viruses make them highly immunogenic, with important immunogenic features like : their size (thus enabling direct draining to the lymph nodes) and their repetitive surface epitope-display[33–37]. In fact, many preclinical studies have shown that high-density and unidirectional antigen-display on CLPs consistently increase the immunogenicity of the presented antigen, and promotes strong and durable antigen-specific antibody responses[38,39]. Importantly, the immune activating properties of the repetitive CLP epitope-display appear to be universally recognized in all mammalian species, including humans[40,41]. Indeed, a strong proof-of-concept in humans has been established by the Human Papillomavirus (HPV) VLP vaccines (Cervarix®, Gardasil®, and Gardasil 9®), which appear to generate lifelong protective antibody responses after a single immunization, an achievement unprecedented by any other recombinant vaccine[42–44]. Finally, the production of AP205 CLPs in *E. coli* is highly scalable and results in encapsulation of bacterial RNA, which act as a potent Th1-type adjuvant through engagement of toll-like receptor (TLR) 7/8 [45].

Here, we describe the design, development and immunogenicity in mice of two CLP-based SARS-CoV-2 RBD vaccines. Two RBD antigen designs were evaluated based on their stability and accessibility to the ACE2 receptor binding epitope, before and after coupling to CLPs. The immunogenicity of the vaccines were assessed in mice, and the neutralization capacity of vaccine-induced immunoglobulins were evaluated using two different clinical SARS-CoV-2 isolates. Together, these data establish a strong proof-of-concept for the CLP-RBD Covid-19 vaccine, which was highly immunogenic and elicited a strong viral neutralizing response. The potential ability of the CLP-platform to promote a strong and focused Th1-type antibody response targeting neutralizing epitopes on the RBD is promising, and supports the further clinical development of the RBD-CLP vaccine. We believe our RBD-CLP vaccine hold the potential to induce a protective immune response in humans, and thus, the lead RBD-CLP vaccine has been forwarded for GMP production and clinical development.

Results

Development and Characterization of a CLP-based SARS-COV-2 Vaccines

The RBD (amino acids (aa) 319-591) of the SARS-CoV-2 spike protein (Sequence ID: QIA20044.1) was genetically fused at either the N- or C-terminus to the split-protein Catcher, used for conjugation to the CLP (Fig. 1A,C). The two RBD antigens (termed RBDn and RBDc, respectively) were expressed in Schneider-2 (ExpreS^2) insect cells, yielding approximately 8 mg/L for transient cell line and 50mg/L for stable cell line. RBDc appeared to be a high-quality monomeric protein (supplementary Fig. 1), and the same was true for RBDn (data not shown). The split-protein peptide Tag was genetically fused to the coat protein of the AP205 and expressed in *E. coli* with yields in the gram per liter range. The recombinant Tag-AP205 protein spontaneously forms CLPs presenting the peptide Tag on its surface[26] (Fig. 1C). Mixing of Catcher-RBD and Tag-CLPs result in the formation of a covalent isopeptide bond between the Catcher and Tag[46–51]. Covalent coupling of the RBD antigens to the CLPs was confirmed by SDS-PAGE analysis, by the appearance of a protein band of 60kDa, corresponding to the added size of the RBD antigen (43 kDa) and Tag-CLP subunit (16.5 kDa) (Fig. 1B, lane 2 and 5). The samples were subjected to a stability spin test (16000g, 2min), showing no loss of the coupling band (60kDa), indicating that the vaccines are stable and not prone to precipitation or aggregation (Fig. 1B, lane 3 and 6). The coupling efficiency of the reactions were assessed by densitometry to be approximately 33% for the RBDc and 45% for the RBDn vaccine. For the RBDc-CLP and RBDn-CLP vaccines, this means that each CLP (build from 180 subunits) was decorated with ~60 RBDc and ~80 RBDn antigens, respectively. The Tag/Catcher mediated conjugation results in unidirectional display of the RBD antigens, thus the positioning of the Catcher on the RBD could affect how the antigen is oriented on the CLP surface (Fig. 1C). However, structural modelling of the RBD-CLP vaccine suggested, that both the N- and C-terminus of the RBD antigen are in close proximity to the CLP surface (Fig. 1D), and that RBD has a similar orientation whether the catcher is attached N- or C terminally. In addition, the modelling suggested that the ACE2 binding epitope on RBD was accessible for immune recognition on the CLPs (Fig. 1D). After removal of unbound RBD, the integrity and aggregation of the vaccines were analyzed by transmission electron microscopy (TEM) and dynamic light scattering (DLS). TEM analysis confirmed the presence of intact CLP-antigen complexes of the expected size for both vaccines (Fig. 2A, C). However, DLS analysis showed that the RBDc-CLP vaccine had propensity for aggregation, as indicated by a high polydispersity (Pd% ~30) and showed evidence of larger aggregates (Fig. 2B). In contrast, the RBDn-CLP vaccine showed little aggregation with a single peak of the expected size of monodisperse CLP antigen complexes (~50nm) (Fig. 2D).

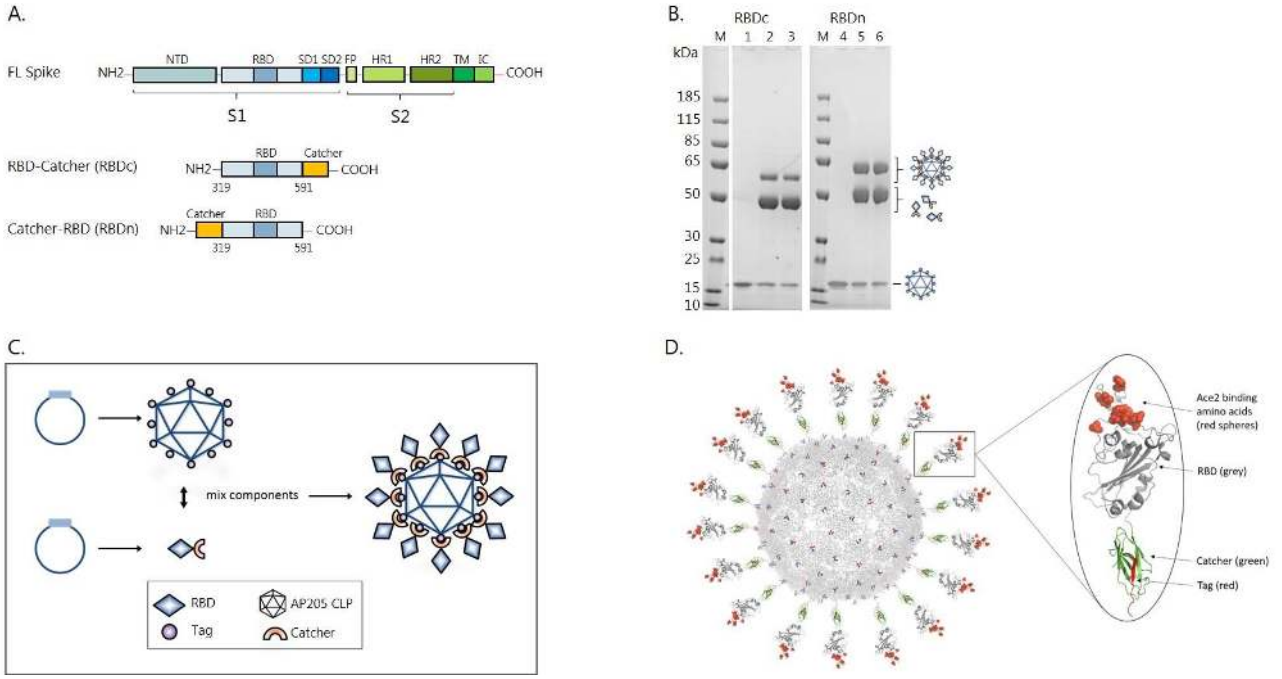

Figure 1 RBD-CLP vaccine design and characterization. (A) Schematic representation of the complete SARS-CoV-2 spike protein including the two RBD-Catcher antigen designs. NTD = N-terminal domain, FL= full-length, RBD = receptor-binding domain, SD1 = subdomain 1, SD2 = subdomain 2, FP = fusion peptide, HR1 = heptad repeat 1, HR2 = heptad repeat 2, TM = transmembrane region, IC = intracellular domain **(B)** Individual vaccine components on a reduced SDS-PAGE. M= marker, lane 1: unconjugated Tag-CLPs (16.5kDa), lane 2: RBDc-CLP conjugation after overnight incubation at 4°C (60kDa), lane 3: RBDc-CLP conjugation after overnight incubation at 4°C (60kDa) + spin test, lane 4: unconjugated Tag-CLPs (16.5kDa), lane 5: RBDn-CLP conjugation after overnight incubation at RT (60kDa), lane 6: RBDn-CLP conjugation after overnight incubation at RT (60kDa) + spin test. **(C)** Schematic representation of the Tag/Catcher-AP205 technology used to create the RBD-CLP vaccines. The genetically fused peptide Tag at the N-terminus of each AP205 capsid protein (total of 180 subunits per CLP) allows unidirectional and high-density coupling of the RBD antigen, via interaction with the N- or C-terminal Catcher (*i.e.* the corresponding binding partner) **(D)** Structural illustration of the RBD-CLP vaccine, based on the SARS-CoV-2 spike (Sequence ID: QIA20044.1), Tag/Catcher (not published), and AP205 CLP (Sequence ID: NP_085472.1)[45] structures. The Tag is shown in red, Catcher in green, RBD in grey with the amino acids residues involved in ACE2 binding interface shown as red spheres.

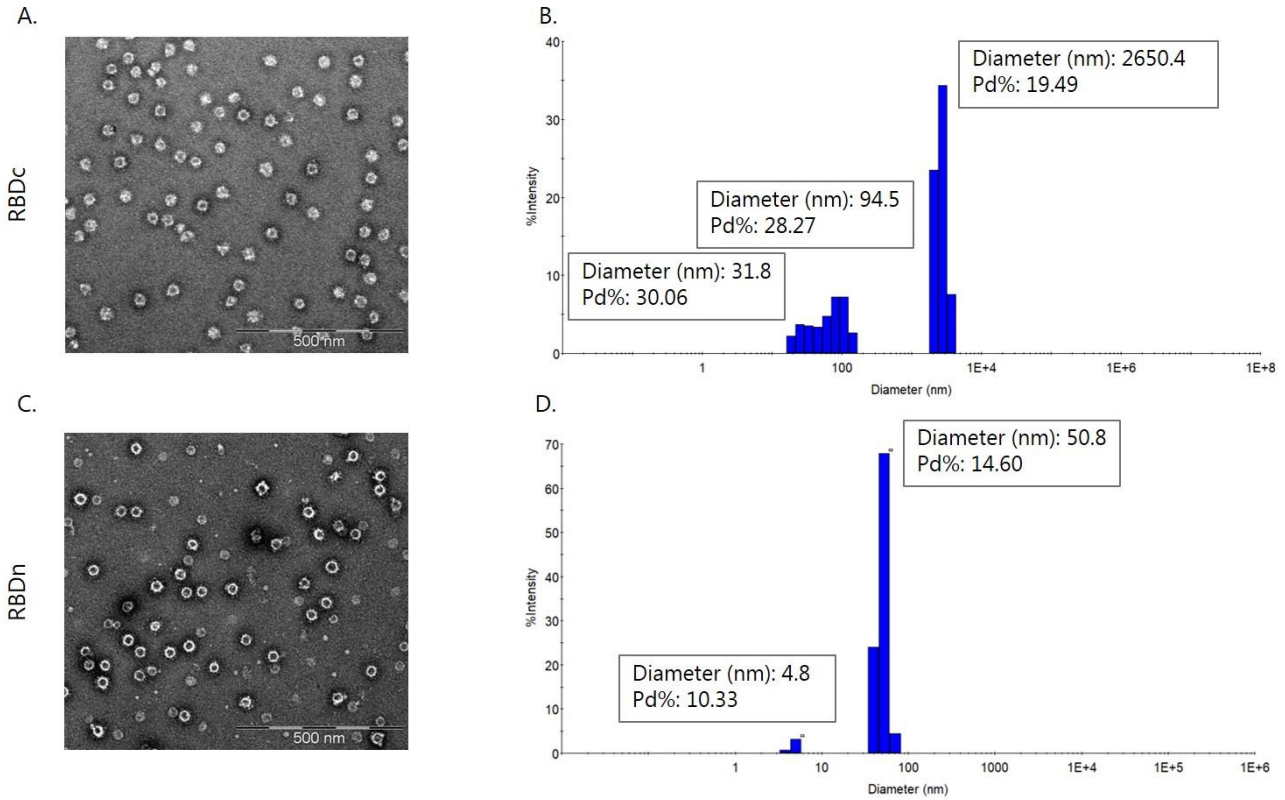

Figure 2 Vaccine quality assessment. (A,C) Transmission electron microscope (TEM) images of the negatively stained purified RBDc-CLP or RBDn-CLP vaccine. Scale bar is 500nm. **(B,D)** Histogram of the % intensity of the purified RBDc-CLP or RBDn-CLP particles from DLS analysis. Annotated are the average diameter and polydispersity (Pd%) for the particles.

Qualification of Antigen structure and CLP-display

The protein fold of the recombinant RBD antigens was validated by measuring their affinity for binding to the human receptor, ACE2. Specifically, the binding affinity to ACE2 was measured for each antigen, before and after coupling to the CLP. Binding of RBDn was performed in a concentration titration series using an Attana Biosensor and showed high affinity binding to immobilized ACE2 with a K_D of 19.4 nM (Fig. 3A), and no binding to a blank reference chip (data not shown). Similar results were shown for RBDc (Supplementary fig. 2A, K_D=34.6 nM). This demonstrates that both RBDc and RBDn have a native structure around the ACE2 binding epitope when expressed as soluble proteins. Importantly, both RBD antigens bound effectively to the ACE2 receptor also when displayed on CLPs (Fig. 3B and Supplementary fig. 2B), thus confirming that the CLP display maintained exposure of the ACE2 binding epitope.

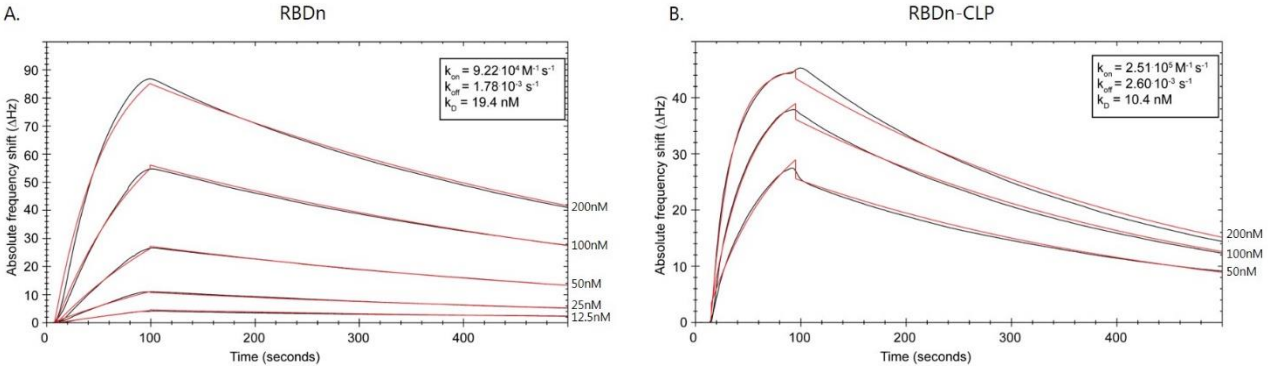

Figure 3 ACE2 binding kinetics for RBDn and RBDn-CLP (A) Real time binding (black curves) of RBDn to immobilized hACE2 on the chip surface. Red curves show theoretical curves obtained using a 1:1 simple binding model. Analyte concentrations are shown to the right and k_{on}, k_{off} and k_D are boxed. **(B)** Real time binding (black curves) of ExpreS^2 produced ACE2 to immobilized RBDn-CLP on the chip surface. Red curves show theoretical curves obtained using a 1:1 simple binding model. Analyte concentrations are shown to the right and k_{on}, k_{off} and k_D are boxed.

Immunogenicity of the RBD-CLP Vaccines

The immunogenicity of the RBD-CLP vaccines (RBDn-CLP and RBDc-CLP) was assessed in BALB/c mice serum, obtained after prime and boost immunizations, and compared to the immunogenicity of soluble equimolar antigen vaccine formulations (RBDn and RBDc). All vaccines were formulated in Squalene-Water-Emulsion (Addavax^{TM}) adjuvant. Antigen-specific IgG titers were measured by ELISA using a recombinant full-length (aa35-1227) SARS-CoV-2 spike protein for capture. Both RBD-CLP vaccines lead to seroconversion in all mice, and booster immunizations distinctly increased the antibody levels (Fig. 4). Furthermore, IgG levels were markedly higher in RBD-CLP vaccinated mice, compared to mice vaccinated with the soluble protein ($p=<0.05$) (Fig. 4).

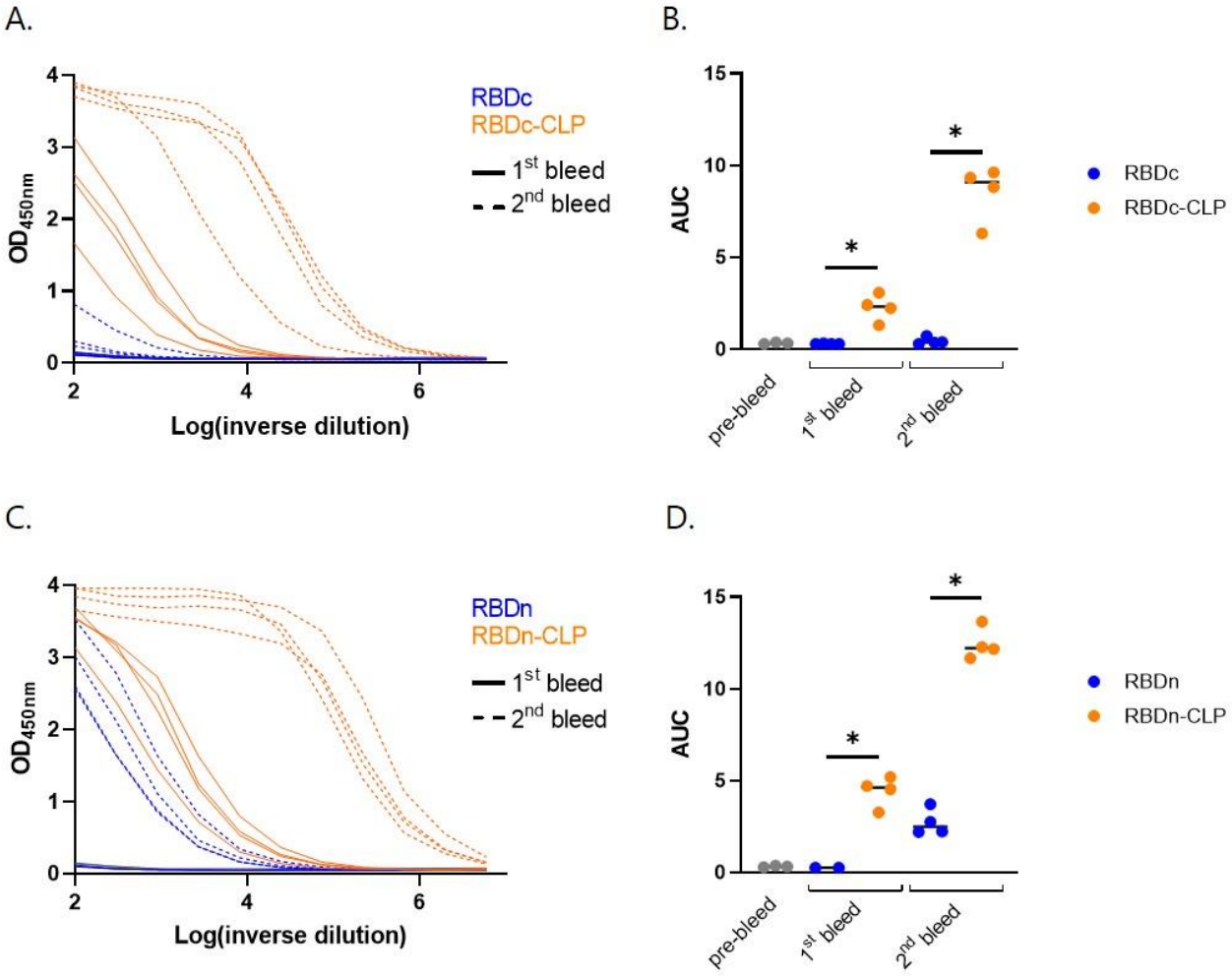

171

172 **Figure 4 RBD-CLP vaccines induce high antigen-specific antibody titers in mice. (A)** Dilution curves from ELISA of total anti-SARS-
173 CoV-2 spike (aa35-1227) IgG antibodies detected in sera from BALB/c mice (n=4) immunized intramuscularly with soluble RBDc (prime
174 2µg / boost 2µg) or CLP-displayed RBDc (RBDc-CLP) (prime 1µg / boost 1µg). Analyzed sera was obtained before vaccination (pre-
175 bleed), two weeks after the prime (1st bleed) or boost (2nd bleed) vaccinations. **(B)** ELISA results depicted in the form of area under
176 curve (AUC), the bars represent the median. Non-parametric Mann-Whitney test was used for statistical comparison. A statistically
177 significant ($p < 0.05$) differences are marked by the *. **(C)** Dilution curves from ELISA of total anti-SARS-CoV-2 spike (aa35-1227) IgG
178 antibodies detected in sera from Balb/c mice (n=4) immunized intramuscularly with soluble RBDn-Catcher (prime 5µg / boost 5µg)
179 or CLP-displayed RBDn (RBDn-CLP) (prime 6.5µg / boost <0.1µg / boost 6.5µg). Analyzed sera was obtained before vaccination (pre-
180 bleed), two weeks after the prime (1st bleeds) or after boost-boost (2nd bleed) vaccinations. **(D)** ELISA results depicted in the form of
181 AUC, the bars represent the median. Non-parametric Mann-Whitney test was used for statistical comparison. A statistically significant
182 ($p < 0.05$) differences are marked by the *.

183

184 ## Neutralization capacity of vaccine-induced anti-RBD antibodies

185 The capacity of the vaccine-induced mouse antibodies to neutralize SARS-CoV-2 virus was measured *in vitro*
186 by two different external laboratories, by testing the capacity of two different clinical SARS-CoV-2 isolates to
187 infect humanized VeroE6 cells. The serum from mice immunized with RBDc-CLP showed significantly higher
188 neutralization capacity than serum from mice immunized with soluble RBDc (Fig. 5A, supplementary fig.3,
189 5A). Furthermore, after the first immunization with the RBDn-CLP vaccine, serum exhibited a 100%

neutralization titer at a serum dilution of 1:80 (Fig. 5B). Following booster immunizations, serum from these mice showed 100% neutralization even at a dilution of 1:10240 (Fig. 5C, supplementary fig. 4). Similar results were obtained using a different clinical SARS-CoV-2 isolate, (Supplementary fig. 5). A correlation analysis between the ELISA antibody titers and neutralization capacity, showed that there was a positive correlation between these measurements (Ks=0.7152, p=0.0461) in mice immunized with the CLP vaccines, but not in the mice vaccinated with soluble RBD (Ks= 0.316, p=0.4679) (Fig. 5D). The virus neutralization capacity was also evaluated for human serum from individuals having recovered from COVID-19 (Fig. 6A). Prior to this analysis, serum samples were grouped based on having either 'very high' or 'low' ELISA titers for SARS-CoV-2 binding capacity (*i.e.* >400 or ≤400 end-point titer, respectively) (data not shown). The serum from mice receiving multiple immunizations with the RBDn-CLP vaccine showed markedly higher virus neutralization activity compared to the serum from any of the sera from patients recovered from COVID-19. However, serum from mice immunized once with RBDn-CLP showed similar neutralizing activity than the 'high' patient sera (Fig. 6B). Samples from patients with 'high' ELISA titers exhibited higher virus neutralization activity than samples from patients with 'low' ELISA titers (p=0.0025) (Fig. 6B). Together these data establish a strong proof-of-concept for the capacity of the RBDn-CLP vaccine to elicit a strong antibody response targeting neutralizing epitopes in the RBD of the SARS-CoV-2 spike protein.

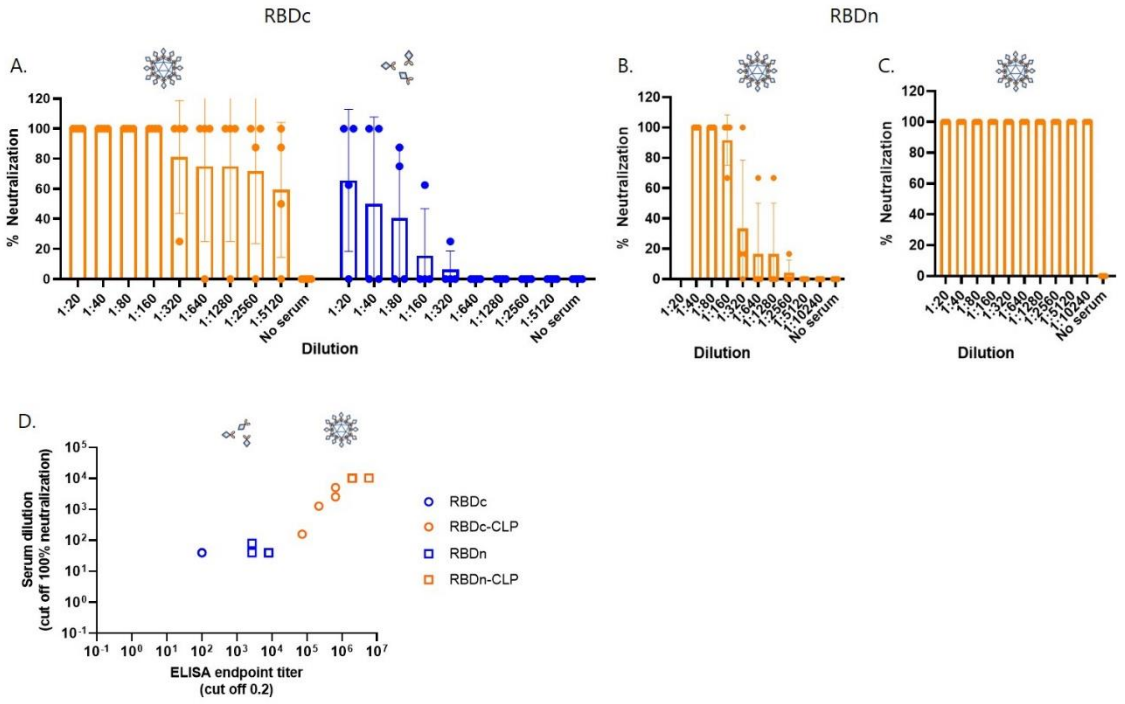

Figure 5 Serum from mice immunized with RBD-CLP vaccines neutralize SARS-CoV-2 *in vitro*. (A) Serum from mice immunized and boosted with RBDc-CLP (orange) (prime 1µg / boost 1µg) or soluble RBDc (blue) (prime 2µg / boost 2µg) was mixed with a SARS-CoV-

2 virus and tested for cell entry. Each dot represents the percentage neutralization per mouse per dilution. Bars represent the mean and SD. **(B, C)** Serum from mice immunized with RBDn-CLP (prime 6.5µg / boost <0.1µg / boost 6.5µg) from first bleed after the first immunization (B) or second bleed after the booster immunizations (C), was mixed with a SARS-CoV-2 virus and tested for cell entry. Each dot represents the percentage neutralization per mouse per dilution. Bars represent the mean and SD. **(D)** Correlation between IgG endpoint titer (2nd bleed, cutoff 0.2) and serum dilution required for 100% virus neutralization. Endpoint titers were determined from dilution curves, by ELISA, from sera of mice immunized with RBDc (prime 2µg / boost 2µg), RBDc-CLP (prime 1µg / boost 1µg), RBDn (prime 5µg / boost 5µg) or RBDn-CLP (prime 6.5µg / boost <0.1µg / boost 6.5µg) and correlated to the serum dilution required for 100% virus neutralization in the neutralization assay done on the same sera. Each dot represents one mouse. Pearson r Non- test was used to assess correlation.

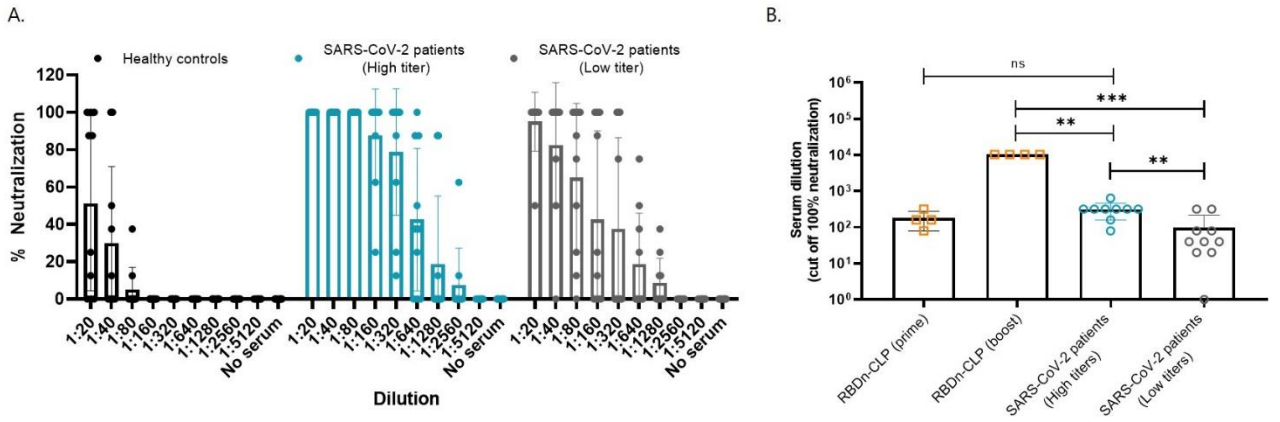

Figure 6 Neutralization capacity of serum from convalescent SARS-CoV-2 patients. (A) A dilution series of individual human plasma samples from SARS-CoV-2 patients (with either 'high' or 'low' ELISA binding titer against SARS-CoV-2 spike protein) or healthy controls were mixed with a clinical SARS-CoV-2 isolate and tested for cell entry. Each dot represents the percentage neutralization per sample, per dilution. Bars represent the mean of the group with a standard deviation. **(B)** Endpoint serum dilution required for 100% virus neutralization. Each dot represents the serum dilution needed for 100% virus neutralization according to the dilution titration of the sera in the neutralization assay (Fig. 6A and Fig. 5B,C). Bars represent the mean of the group with a standard deviation. Mann-Whitney test was used for statistical comparison. Statistically significant differences are marked by asterisk: ns=non-significant, **: p≤0.005, ***: p≤0,001.

Discussion

In less than six months, more than 12 million confirmed cases of SARS-CoV-2 infection, and more than 550,000 COVID-19 related deaths have been reported[52]. Thus, development of an effective vaccine is of high priority worldwide. The ideal SARS-CoV-2 vaccine should be safe, and capable of activating a long-term protective immune response. High immunogenicity is pivotal for vaccine efficacy and represents a fundamental challenge for the vaccine development[53]. In the context of COVID-19, the elderly carry an increased risk of serious illness[54], but it is also well known that this group generally responds less effectively to vaccination[55,56]. In addition, the balance between immunogenicity and safety vary among different vaccine platforms, and concerns have been raised that some SARS-CoV-2 vaccines can potentially cause enhanced disease. This risk is believed to be higher for vaccines which fail to induce a sufficiently strong virus neutralizing antibody response[57]. Although it is still unclear whether natural infection with SARS-CoV-2 can

induce long-term protective immunity, natural infection with members of the coronavirus family causing common cold, provide only short-term protection[58–60]. Accordingly, COVID-19 vaccines may need to induce a stronger and more durable effective immune response than natural infection, in order to provide long term protection.

Our strategy for developing a CLP-based COVID-19 vaccine displaying the SARS-CoV-2 spike RBD holds several potential advantages. Firstly, other CLP-based vaccines have shown to be safe and highly immunogenic in humans. In fact, the marketed Human Papillomavirus (HPV) vaccines, based on HPV L1 CLP, induce extremely potent and durable antibody responses otherwise only seen after vaccination with live-attenuated viral vaccines[42–44]. With regard to safety, several experts have stated that SARS-CoV-2 vaccines should preferentially induce a high level of neutralizing antibodies, while avoiding activation of Th2 T-cells, to reduce the risk of eosinophil-associated immunopathology following infection after SARS-CoV-2 vaccination [57,61]. To this end, it seems ideal that production of AP205 CLPs in *E. coli* results in encapsulation of bacterial host cell RNA, promoting Th1 type responses by activation of TLR7/8[45]. Additionally, a recent review[53], comparing different SARS-CoV-2 vaccine candidates, suggests that recombinant proteins and nanoparticles are the preferred option for obtaining high safety, high immunogenicity and hold potential for raising neutralizing antibody titers. Thus, the strategy of targeting only the RBD of the SARS-CoV-2 spike protein, along with the unique ability of the Tag/Catcher-AP205 platform to present the RBD in a high-density and unidirectional manner, may not only ensure high immunogenicity, but may also enable induction of responses with a high proportion of neutralizing compared to binding antibodies[9–15]. In fact, the unidirectional antigen display enabled by the Tag/Catcher-AP205 platform has previously been exploited to selectively favor induction of antibodies targeting desired epitopes[62]. It is thus encouraging that both our RBD-CLP vaccine candidates appear to expose the ACE2 binding epitope, as evidenced by the strong binding of RBD-CLP complexes to ACE2. Our data, comparing the immunogenicity of soluble versus CLP-displayed RBD antigens in mice, show a remarkable effect of the CLP display (approx. 5 fold difference). Indeed, the observed low intrinsic immunogenicity of the soluble RBD antigen even in the presence of Addavax™ adjuvant, emphasizes the need of an effective vaccine delivery platform, and raises concern whether vaccines based on soluble recombinant proteins will be sufficiently immunogenic in humans. Further analysis of the neutralizing capacity vaccine-induced mouse antibodies showed that RBD-CLP vaccines also elicited antibody responses with significantly higher neutralization capacity. This result may not only be due to increased immunogenicity of the CLP-displayed RBD antigen, but could also reflect a higher proportion of neutralizing antibodies in the total pool of vaccine-induced antibodies. Indeed, a strong positive correlation was observed between vaccine-induced antibody titers and virus neutralization activity among the RBD-CLP immunized mice. A

similar correlation was not seen for the soluble RBD vaccines. Serum samples from convalescent patients showed similar neutralization titers as those measured for mouse sera obtained after a prime immunization of RBDn-CLP. A recent review, compiling all the latest data on SARS-CoV-2 vaccine development, suggests that a >50% neutralizing titers at an endpoint titer dilution of 100-500 would be needed to confer protection[53]. In relation to this, our RBDn-CLP vaccine induces 100% neutralization at our highest tested serum dilution >10,000 (or >2560, supplementary fig. 5B), suggesting that it could have the potential to trigger a robust immune response in humans.

To this date, many studies have shown that both genetic and protein-based vaccines need to be supported by a stronger vaccine platform or adjuvant to enable sufficiently potent immune responses[63,64]. Indeed, when looking at emerging data on SARS-CoV-2 vaccine development, it appears that the vaccines that are fast to produce (*i.e.* genetic and virus vectors) might not be able to elicit antibody titers sufficient to confer long lived protection[53]. Additionally, vaccines have many times failed due to low immunogenicity when testing in human clinical trials, despite having produced encouraging results in preclinical models[65,66]. Thus, in the case of SARS-CoV-2, it seems that recombinant proteins or killed/attenuated virus vaccines would most likely be the ones enabling responses strong enough for protection[53]. However, killed or live-attenuated viruses has potential safety concerns. Thus, we propose that the Tag/Catcher-AP205 system is an ideal platform for delivery of the RBD antigen, to enable induction of a strong, long-lasting and highly neutralizing antibody response, while avoiding high safety risks. Specifically, the intrinsic CLP properties provide the perfect balance between high immunogenicity and complete safety, which is of main importance for a vaccine supposed to protect globally, including the at risk populations. Based on these results, the RBDn-CLP vaccine has been selected as our lead candidate, due to its high stability and low aggregation compared to RBDc-CLP, as well as its high immunogenicity and neutralizing capacities, in mice. Thus, this vaccine has been transferred to GMP, with a planned phase 1 clinical testing in Germany (funded by H2020).

Methods

Design, expression and purification of recombinant proteins

RBD antigens were designed with boundaries aa319-591 of the SARS-CoV-2 sequence (Sequence ID: QIA20044.1). The RDB antigens were genetically fused with the split-protein "Catcher" at the N-terminus or the C-terminus (referred to as RBDn and RBDc, respectively). Both antigen constructs had an N-terminally BiP secretion signal and a C-terminal C-tag (N-RBD-EPEA-C) used for purification. A GSGS linker was inserted between the RBD and the Catcher. The final gene sequences were codon optimized for expression in *Drosophila melanogaster* and were synthesized by Geneart©. The ExpreS^2 platform was used to produce all proteins by transient transfection. Briefly, Schneider-2 (ExpreS^2) cells were transiently transfected using transfection reagent (ExpreS^2 Insect TRx5, ExpreS^{2}ion Biotechnologies) according to manufacturer's protocol. Cells were grown at 25°C in shake flask for 3 days before harvest of the supernatant containing the secreted protein of interest. Cells and debris were pelleted by centrifugation (5000rpm for 10 minutes at 4°C) in a Beckman Avanti JXN-26 centrifuge equipped with a JLA 8.1000 swing-out rotor. The supernatant was decanted and passed through a 0.22 µm vacuum filter (PES) before further processing. The supernatant was passed over a Centramate tangential flow filtration (TFF) membrane (0.1m^2, 10kDa MWCO, PALL) mounted in a SIUS-LS filter holder atop a SIUS-LS filter plate insert (Repligen/TangenX). The retentate was concentrated ten-fold by recirculation through a concentration vessel of 1 litre volume without stirring. Buffer exchange was performed by diafiltration until achieving a turn-over-volume of 10.

The crude protein was loaded onto a Capture Select C tag resin (Thermo Fisher) affinity column and washed with capture buffer (25mM Tris-HCl, 100mM NaCl, pH7.5). The captured protein was step-eluted in 25 mM Tris-HCl (pH7.5) containing increasing concentrations of $MgCl_2$ (0.25M, 0.5M, 1M and 2M). Fractions containing the protein of interest were pooled and concentrated (Amicon 15ml, 10kDa or 30kDa MWCO). Concentrated protein was loaded onto a preparative Superdex-200pg 26/600 (Cytiva) SEC column equilibrated in 1x PBS (Gibco) and eluted in the same buffer. Fractions containing the monomer RBD protein were pooled and concentrated as above. The ACE2 protein (aa1–615) and the spike protein (aa.35-1227)-Ctag (ΔTM-ΔFurin-CoV-PP-Ctag)) were N-terminally tagged with a BiP secretion signal and a C-terminal Twin-Strep-tag (Iba, GmbH) affinity-tag. The crude protein was loaded onto a StreptactinXT (IBA) affinity column. Proteins were eluted using capture buffer (100mM Tris-HCl, 150mM NaCl, 1 mM EDTA pH 8.0) supplemented with 50mM D-Biotin (BXT buffer, Iba GmbH)

Design, expression and purification of Tag-CLP

The proprietary peptide binding Tag and a linker (GSGTAGGGSGS) was added to the N-terminus of the *Acinetobacter phage* AP205 coat protein (Gene ID: 956335) by PCR. The gene sequence was inserted into the

pET28a(+) vector (Novagen) using *NcoI* (New England Biolabs) and *NotI* (New England Biolabs) restriction sites. The Tag-CLP was expressed and purified as previously described for Spy-AP205 CLPs[26].

Formulation and purification of the RBD-CLP vaccines

The Tag-CLP and the RBDc antigen were mixed in a 1:2 molar ratio in 100mM Bis-Tris, 250mM NaCl (pH 6.5) buffer overnight at 4oC. Tag-CLP and RBDn antigen were mixed in a 1:1 molar ratio in 1xPBS, 5% glycerol and incubated overnight at room temperature. Different working buffers for RBDn and RBDc vaccines were selected according to a buffer screen to ensure vaccine stability (not shown). A subsequent buffer screen showed that the RBDn-CLP was stabilized by the addition of different sugars (sucrose, xylitol and trehalose). Accordingly, PBS buffer, pH 7.4, supplemented by 400mM xylitol was chosen for quality assessment of the RBDn vaccine. The mixture of RBD and CLP was subjected to a "spin test" to assess stability. Specifically, a fraction of the sample was spun at 16000g for 2min, and equal amounts of pre- and post-spin samples were subsequently loaded on a reduced SDS-PAGE to assess potential loss in the post-spin sample due to precipitation of aggregated RBD-CLP complexes. The RBD-Catcher coupling efficiency was calculated as percentage conjugation (i.e. number of bound antigens divided by the total available binding sites (=180) per CLP) by densitometric analysis of on the SDS-PAGE gel, using ImagequantTL (as previously described[67]. In parallel, RBDc-CLP was purified by density gradient ultracentrifugation by adding the RBDc-CLP onto an Optiprep™ step gradient (23, 29 and 35%) (Sigma-Aldrich) followed by centrifugation for 3.30h at 47800rpm, as previously described26. The conjugated RBDn-CLP was purified by dialysis (cutoff 1000kDa) in a 1xPBS with 5% (v/v) glycerol for immunization studies or 400mM xylitol for quality assessment.

Quality assessment of the RBD-CLP vaccines

Purified RBD-CLP were both quality checked by negative stain Transmission electron microscopy (TEM) (detailed description 10.1038/s41598-019-41522-5) as well as by Dynamic Light Scattering (DLS) analysis (DynaPro Nanostar, Wyatt technology). For DLS analysis, the RBD-CLP sample was first spun at 21,000 g for 2.5 minutes and then loaded into a disposable cuvette. The sample was then run with 20 acquisitions of 7 seconds each. The estimated diameter of the RBD-CLP particle population and the percent polydispersity (%Pd) was calculated by Wyatt DYNAMICS software (US).

ACE2 binding kinetics by Attana© Biosensor

Kinetic interaction experiment of RBD antigens and CLP-RBD binding to hACE2 were performed using a biosensor QCM Attana A200 instrument (Attana AB). hACE2 (50µg/ml) or VLP-RBDn (50µg/ml) were immobilized on a LNB carboxyl chip by amine coupling using EDC and S-NHS chemistry following manufacturer's instructions. A non-coated LNB chip was used as reference. Two-fold dilution series of RBDc

(200nM-6.25nM) and RBDn (200nM-12.5nM) were prepared in 1xPBS pH 7.4. ExpreS^2 produced hACE2 (200nM-50nM) was prepared in 1xPBS+400mM xylitol pH7.4 running buffer. All sensorgrams were recorded at 25µl/min at 22°C using an 84 s association and 3000 s dissociation time to allow complete baseline recovery. The absolute change in frequency (ΔHz) during association and dissociation were analyzed using Attester Evaluation software (Attana AB). Injection of running buffer (background binding) was subtracted for each sensorgram prior to fitting k_{on} and k_{off}. The kinetic parameters were calculated using a 1:1 binding model using TraceDrawer software (Ridgeview Instruments AB).

ACE2 binding to RBD-CLP by ELISA

RBDc-CLP binding to ACE2 was performed using an enzyme-linked immune-sorbent assay (ELISA). 96-well plates (Nunc MaxiSorp) were coated overnight at 4°C with 0.05µg/well recombinant ACE2 produced in ExpreS^2 cells. Plates were blocked for 1 hour at room temperature (RT) using 0.5% skimmed milk in PBS. 2,5ug purified RBDc-CLP was added per well, or CLP alone and RBD alone as controls and incubated for 1h at RT. Plates were washed three times in PBS between each step. Mouse monoclonal antibody (produced in-house), detecting AP205 was diluted 1:10,000 in blocking buffer, followed by incubation for 1 hour at RT. Horseradish peroxidase (HRP) conjugated goat anti-mouse IgG (Life technologies, A16072) was diluted 1:1000 in blocking buffer followed by 1 hour incubation at RT. Plates were developed with TMB X-tra substrate (Kem-En-Tec, 4800A) and absorbance was measured at 450nM.

Mouse immunization studies

Experiments were authorized by the National Animal Experiments Inspectorate (Dyreforsøgstilsynet, license no. 2018-15-0201-01541) and performed according to national guidelines. 12-14 weeks old female BALB/c mice (Janvier, Denmark) were immunized intramuscularly, in the thigh, with either 2µg free RBDc antigen (1x PBS, pH7.4) (N=4) or 1µg CLP-displayed RBDc (PBS with Optiprep™) (N=4), using a two-week interval prime-boost regimen. For the RBDn study, mice were immunized with a dose of 5µg free RBDn antigen (1x PBS, pH7.4) or 6.5µg CLP-displayed RBDn (1xPBS, pH7.4, 5% glycerol) (N=4) and boosted 2 weeks later with 5µg free RBDn antigen (1x PBS, pH7.4) or 0.1µg CLP-displayed RBDn (1xPBS, pH7.4, 5% glycerol) (N=4). Considering the low dose used for the RBDn-CLP boost, it was decided to give them an extra boost a week later (3 weeks post prime) with 6.5µg CLP-displayed RBDn (1xPBS, pH7.4, 5% glycerol) (N=4). For both studies, the concentration of the antigen displayed on the CLP was calculated by densitometric measurement (ImageQuant TL), using a protein concentration ladder as a reference. All vaccines were formulated using Addavax™ (Invivogen). Blood samples were collected prior to the first immunization (pre-bleed) as well as two weeks after each immunization. Serum was isolated by spinning the blood samples down for 8min at 800 g, 8°C. This procedure was repeated twice.

Analysis of vaccine-induced antibody responses

Antigen-specific total IgG titers were measured by enzyme-linked immune-sorbent assay (ELISA). 96-well plates (Nunc MaxiSorp) were coated overnight at 4°C with 0.1µg/well recombinant ExpreS^2 produced SARS-CoV-2 Spike (35-1227) protein in PBS. Plates were blocked for 1 hour at room temperature (RT) using 0.5% skimmed milk in PBS. Mouse serum was diluted 1:100 in blocking buffer, and added to the plate in a 3-fold dilution, followed by incubation for 1 hour at RT. Plates were washed three times in PBS in between steps. In order to measure total serum IgG, Horseradish peroxidase (HRP) conjugated goat anti-mouse IgG (Life technologies, A16072) was diluted 1:1000 in blocking buffer followed by 1 hour incubation at RT. Plates were developed with TMB X-tra substrate (Kem-En-Tec, 4800A) and absorbance was measured at 450nM.

Virus Neutralization assay (University of Aarhus, Denmark)

SARS-CoV2, Freiburg isolate, FR-4286 (kindly provided by Professor Georg Kochs, University of Freiburg) was propagated in VeroE6 expressing cells expressing human TMPRSS2 (VeroE6-hTMPRSS2) (kindly provided by Professor Stefan Pöhlmann, University of Göttingen)[68] with a multiplicity of infection (MOI) of 0.05. Supernatant containing new virus progeny was harvested 72h post infection, and concentrated on 100kDa Amicon ultrafiltration columns (Merck) by centrifugation for 30 minutes at 4000 g. Virus titer was determined by $TCID_{50\%}$ assay and calculated by Reed-Muench method[69]. Sera from immunized mice or human serum/plasma (kindly provided by Herlev Hospital and Rigshospitalet, Denmark) were heat-inactivated (30 min, 56 °C), and prepared in a 2-fold serial dilutions in DMEM (Gibco) + 2% FCS (Sigma-Aldrich) + 1% Pen/Strep (Gibco) + L-Glutamine (Sigma-Aldrich). Sera were mixed with SARS-CoV-2 at a final titer of 100 $TCID_{50}$/well, and incubated at 4˚C overnight. A "no serum" and a "no virus" (uninfected) control samples were included. The following day virus:serum mixtures were added to 2 x 10^4 Vero E6 TMPRSS2 cells seeded in flat-bottom 96-well plates, and incubated for 72h in a humidified CO_2 incubator at 37 ˚C, 5% CO_2, before fixing with 5% formalin (Sigma-Aldrich) and staining with crystal violet solution (Sigma-Aldrich). The plates were read using a light microscope (Leica DMi1) with camera (Leica MC170 HD) at 4x magnification, and cytopathic effect (CPE) scored.

Virus Neutralization assay (University of Leiden, Netherlands)

SARS-CoV-2 (Leiden-001 isolate, unpublished) was propagated and titrated in Vero E6 cells [CRL-1580, American Type Culture Collection (ATCC)] using the tissue culture infective dose 50 ($TCID_{50}$) endpoint dilution method and the $TCID_{50}$ was calculated by the Spearman-Kärber algorithm[70]. Neutralization assays against live SARS-CoV-2 were performed using the virus micro-neutralization assay. Briefly, Vero-E6 cells were seeded at 10000cells/well in 96-well tissue culture plates 1 day prior to infection. Serum samples were heat-inactivated at 56ºC for 30 minutes and prepared in a 2-fold serial dilutions (1:10-1280) in 60µL EMEM (Lonza)

supplemented with 1% pen/strep (Sigma-Aldrich, P4458), 2mM L-glutamine (PAA) and 2% FCS (Bodinco BV). Diluted sera were mixed with equal volumes of 120 TCID50/60µL SARS-CoV-2 and incubated for 1h at 37 °C. The virus:serum mixtures were then added onto Vero-E6 cell monolayers and incubated at 37 °C in a humidified atmosphere with 5 % CO_2. Cells either unexposed to the virus or mixed with 120 TCID50/60µL SARS-CoV-2 were used as negative (uninfected) and positive (infected) controls, respectively. 3 days post-infection, cells were fixed and inactivated with 40µL 37% formaldehyde/PBS solution/well overnight at 4 °C. Cells were then stained with crystal violet solution 50µL/well, incubated for 10 minutes and rinsed with water. Dried plates were evaluated for viral cytopathic effect and the serum neutralization titer was determined as the reciprocal value of the highest dilution resulting in completely inhibiting virus-induced cytopathogenic effect. For the purpose of graphical representation, samples with undetectable antibody titers were assigned values two-fold lower than the lowest detectable titer (titer 10), which corresponds to the nearest dilution that could not be measured (titer 5). A SARS-CoV-2 back-titration was also included with each assay run to confirm that the dose of the used inoculum was within the acceptable range of 30 to 300 $TCID_{50}$.

References

1. WHO/Europe | Coronavirus disease (COVID-19) outbreak - 2019-nCoV outbreak is an emergency of international concern. Available at: https://www.euro.who.int/en/health-topics/health-emergencies/coronavirus-covid-19/news/news/2020/01/2019-ncov-outbreak-is-an-emergency-of-international-concern. (Accessed: 7th July 2020)

2. Lu, R. *et al.* Genomic characterisation and epidemiology of 2019 novel coronavirus: implications for virus origins and receptor binding. *Lancet* **395**, 565–574 (2020).

3. Chen, J. *et al.* Receptor-binding domain of SARS-Cov spike protein: Soluble expression in E.coli, purification and functional characterization. *World J. Gastroenterol.* **11**, 6159–6164 (2005).

4. Yan, R. *et al.* Structural basis for the recognition of SARS-CoV-2 by full-length human ACE2. *Science (80-.).* **367**, 1444–1448 (2020).

5. Chen, Y., Liu, Q. & Guo, D. Emerging coronaviruses: Genome structure, replication, and pathogenesis. *J. Med. Virol.* **92**, 418–423 (2020).

6. Chen, Y., Guo, Y., Pan, Y. & Zhao, Z. J. Structure analysis of the receptor binding of 2019-nCoV. *Biochem. Biophys. Res. Commun.* **525**, 135–140 (2020).

7. Tai, W. *et al.* Characterization of the receptor-binding domain (RBD) of 2019 novel coronavirus: implication for development of RBD protein as a viral attachment inhibitor and vaccine. *Cell. Mol. Immunol.* **17**, 613–620 (2020).

8. Du, L. *et al.* The spike protein of SARS-CoV - A target for vaccine and therapeutic development. *Nat. Rev. Microbiol.* **7**, 226–236 (2009).

9. Cao, Y. *et al.* Potent Neutralizing Antibodies against SARS-CoV-2 Identified by High-Throughput Single-Cell Sequencing of Convalescent Patients' B Cells. *Cell* **182**, 1–12 (2020).

10. Ju, B. *et al.* Human neutralizing antibodies elicited by SARS-CoV-2 infection. *Nature* 1–8 (2020). doi:10.1038/s41586-020-2380-z

11. Pinto, D. *et al.* Cross-neutralization of SARS-CoV-2 by a human monoclonal SARS-CoV antibody. *Nature* 1–6 (2020). doi:10.1038/s41586-020-2349-y

12. Rogers, T. F. *et al.* Rapid isolation of potent SARS-CoV-2 neutralizing antibodies and protection in a small animal model. *bioRxiv* 2020.05.11.088674 (2020). doi:10.1101/2020.05.11.088674

13. Seydoux, E. *et al.* Characterization of neutralizing antibodies from a SARS-CoV-2 infected individual. *bioRxiv* 2020.05.12.091298 (2020). doi:10.1101/2020.05.12.091298

14. Zost, S. J. *et al.* Potently neutralizing human antibodies that block SARS-CoV-2 receptor binding and protect animals. *bioRxiv Prepr. Serv. Biol.* 2020.05.22.111005 (2020). doi:10.1101/2020.05.22.111005

15. Lan, J. *et al.* Structure of the SARS-CoV-2 spike receptor-binding domain bound to the ACE2 receptor. *Nature* 1–8 (2020). doi:10.1038/s41586-020-2180-5

16. Corbett, K. S. *et al.* SARS-CoV-2 mRNA Vaccine Development Enabled by Prototype Pathogen Preparedness. *bioRxiv* 2020.06.11.145920 (2020). doi:10.1101/2020.06.11.145920

17. Smith, T. R. F. *et al.* Immunogenicity of a DNA vaccine candidate for COVID-19. *Nat. Commun.* **11**, 2601 (2020).

18. Kim, E. *et al.* Microneedle array delivered recombinant coronavirus vaccines: Immunogenicity and rapid translational development. *EBioMedicine* **55**, 102743 (2020).

19. Doremalen, N. van *et al.* ChAdOx1 nCoV-19 vaccination prevents SARS-CoV-2 pneumonia in rhesus macaques. *bioRxiv* 2020.05.13.093195 (2020). doi:10.1101/2020.05.13.093195

20. Zhu, F.-C. *et al.* Safety, tolerability, and immunogenicity of a recombinant adenovirus type-5 vectored COVID-19 vaccine: a dose-escalation, open-label, non-randomised, first-in-human trial. *Lancet* (2020). doi:10.1016/S0140-6736(20)31208-3

21. Chen, W.-H. *et al.* Yeast-Expressed SARS-CoV Recombinant Receptor-Binding Domain (RBD219-N1) Formulated with Alum Induces Protective Immunity and Reduces Immune Enhancement. *bioRxiv* 2020.05.15.098079 (2020). doi:10.1101/2020.05.15.098079

22. Gao, Q. *et al.* Development of an inactivated vaccine candidate for SARS-CoV-2. *Science (80-.).* eabc1932 (2020). doi:10.1126/science.abc1932

23. Thanh Le, T. *et al.* The COVID-19 vaccine development landscape. *Nat. Rev. Drug Discov.* **19**, 305–306 (2020).

24. Amanat, F. & Krammer, F. SARS-CoV-2 Vaccines: Status Report. *Immunity* **52**, 583–589 (2020).

25. Draft landscape of COVID-19 candidate vaccines. Available at: https://www.who.int/publications/m/item/draft-landscape-of-covid-19-candidate-vaccines. (Accessed: 7th July 2020)

26. Thrane, S. *et al.* Bacterial superglue enables easy development of efficient virus-like particle based vaccines. *J. Nanobiotechnology* **14**, 30 (2016).

27. Brune, K. D. *et al.* Plug-and-Display: decoration of Virus-Like Particles via isopeptide bonds for modular immunization. *Sci. Rep.* **6**, 1–13 (2016).

28. Tan, L. L., Hoon, S. S. & Wong, F. T. Kinetic Controlled Tag-Catcher Interactions for Directed Covalent Protein Assembly. *PLoS One* **11**, 1–15 (2016).

29. Zakeri, B. *et al.* Peptide tag forming a rapid covalent bond to a protein, through engineering a bacterial adhesin. *PNAS* **109**, E690–E607 (2012).

30. Prö Schel, M. *et al.* Probing the potential of CnaB-type domains for the design of tag/catcher systems. doi:10.1371/journal.pone.0179740

31. Pumpens, P. *et al.* The True Story and Advantages of RNA Phage Capsids as Nanotools. *Intervirology* **59**, 74–110 (2016).

32. Mohsen, M., Gomes, A., Vogel, M. & Bachmann, M. Interaction of Viral Capsid-Derived Virus-Like Particles (VLPs) with the Innate Immune System. *Vaccines* **6**, 1–12 (2018).

33. Bachmann, M. F. *et al.* The Influence of Antigen Organization on B Cell Responsiveness. *Science (80-.).* **262**, 1448–1451 (1993).

34. Bachmann, M. F. & Zinkernagel, R. M. The influence of virus structure on antibody responses and virus serotype formation. *Immunol. Today* **17**, 553–558 (1996).

35. Manolova, V. *et al.* Nanoparticles target distinct dendritic cell populations according to their size. *Eur. J. Immunol.* **38**, 1404–1413 (2008).

36. Alexander Titz, B. *et al.* Innate Immunity Mediates Follicular Innate Immunity Mediates Follicular

Transport of Particulate but Not Soluble Protein Antigen. *J. Immunol.* **188**, 3724–3733 (2012).

37. Bachmann, M. F. & Jennings, G. T. Vaccine delivery: a matter of size, geometry, kinetics and molecular patterns. *Nat. Rev. Immunol.* **10**, 787–796 (2010).

38. Jegerlehner, A. *et al.* Regulation of IgG antibody responses by epitope density and CD21-mediated costimulation. *Eur. J. Immunol.* **32**, 3305–3314 (2002).

39. Leneghan, D. B. *et al.* Nanoassembly routes stimulate conflicting antibody quantity and quality for transmission-blocking malaria vaccines. *Nat. Sci. reports* **7**, 1–14 (2017).

40. Bachmann, M. F. & Jennings, G. T. Therapeutic vaccines for chronic diseases: Successes and technical challenges. *Philos. Trans. R. Soc. B Biol. Sci.* **366**, 2815–2822 (2011).

41. Mohsen, M. O., Zha, L., Cabral-Miranda, G. & Bachmann, M. F. Major findings and recent advances in virus–like particle (VLP)-based vaccines. *Semin. Immunol.* **34**, 123–132 (2017).

42. Schiller, J. & Lowy, D. Explanations for the high potency of HPV prophylactic vaccines. *Vaccine* **36**, 4768–4773 (2018).

43. Schiller, J. T., Castellsagué, X. & Garland, S. M. A review of clinical trials of human papillomavirus prophylactic vaccines. *Vaccine* **30**, F123–F138 (2012).

44. De Vincenzo, R., Conte, C., Ricci, C., Scambia, G. & Capelli, G. Long-term efficacy and safety of human papillomavirus vaccination. *Int. J. Womens. Health* **6**, 999–1010 (2014).

45. Shishovs, M. *et al.* Structure of AP205 Coat Protein Reveals Circular Permutation in ssRNA Bacteriophages. *J. Mol. Biol.* **428**, 4267–4279 (2016).

46. Li, L., Fierer, J. O., Rapoport, T. A. & Howarth, M. Structural Analysis and Optimization of the Covalent Association between SpyCatcher and a Peptide Tag. *J. Mol. Biol.* **426**, 309–317 (2014).

47. Fierer, J. O., Veggiani, G. & Howarth, M. SpyLigase peptide-peptide ligation polymerizes affibodies to enhance magnetic cancer cell capture. *Proc. Natl. Acad. Sci. U. S. A.* **111**, E1176–E1181 (2014).

48. Hatlem, D., Trunk, T., Linke, D. & Leo, J. C. Catching a SPY: Using the SpyCatcher-SpyTag and related systems for labeling and localizing bacterial proteins. *Int. J. Mol. Sci.* **20**, 1–19 (2019).

49. Buldun, C. M., Jean, J. X., Bedford, M. R. & Howarth, M. SnoopLigase Catalyzes Peptide-Peptide Locking and Enables Solid-Phase Conjugate Isolation. *J. Am. Chem. Soc.* **140**, 3008–3018 (2018).

50. Pröschel, M. *et al.* Probing the potential of CnaB-type domains for the design of tag/catcher systems. *PLoS One* **12**, 1–26 (2017).

51. Keeble, A. H. *et al.* Approaching infinite affinity through engineering of peptide–protein interaction. *PNAS* 1–11 (2019). doi:10.1073/pnas.1909653116

52. Coronavirus Update (Live): 11,756,506 Cases and 541,086 Deaths from COVID-19 Virus Pandemic - Worldometer. Available at: https://www.worldometers.info/coronavirus/?utm_campaign=homeAdvegas1? . (Accessed: 7th July 2020)

53. Moore, J. P. & Klasse, P. J. SARS-CoV-2 vaccines: 'Warp Speed' needs mind melds not warped minds. *J. Virol.* (2020). doi:10.1128/JVI.01083-20

54. Wang, L. *et al.* Coronavirus disease 2019 in elderly patients: Characteristics and prognostic factors based on 4-week follow-up. *J. Infect.* **80**, 639–645 (2020).

55. Antia, A. *et al.* Heterogeneity and longevity of antibody memory to viruses and vaccines. *PLOS Biol.* 1–15 (2018). doi:10.1371/journal.pbio.2006601

56. Amanna, I. J. Balancing the efficacy and safety of vaccines in the elderly. *Open Longev. Sci.* **6**, 64–72 (2012).

57. Lambert, P. H. *et al.* Consensus summary report for CEPI/BC March 12–13, 2020 meeting: Assessment of risk of disease enhancement with COVID-19 vaccines. *Vaccine* **38**, 1–8 (2020).

58. Kellam, P. & Barclay, W. The dynamics of humoral immune responses following SARS-CoV-2 infection and the potential for reinfection. *J. Gen. Virol.* jgv001439 (2020). doi:10.1099/jgv.0.001439

59. Cao, W.-C., Liu, W., Zhang, P.-H., Zhang, F. & Richardus, J. H. Disappearance of Antibodies to SARS-Associated Coronavirus after Recovery. *N. Engl. J. Med.* **357**, 1162–1163 (2007).

60. Vabret, N. *et al.* Immunology of COVID-19: Current State of the Science. *Cell Press Immun.* **52**, 910–941 (2020).

61. Simon, H.-U., Karaulov, A. V. & Bachmann, M. F. Strategies to Prevent SARS-CoV-2-Mediated Eosinophilic Disease in Association with COVID-19 Vaccination and Infection. *Int. Arch. Allergy Immunol.* 1–5 (2020). doi:10.1159/000509368

62. Escolano, A. *et al.* Immunization expands B cells specific to HIV-1 V3 glycan in mice and macaques. *Nature* **570**, 468–473 (2019).

63. Podda, A. The adjuvanted influenza vaccines with novel adjuvants: Experience with the MF59-adjuvanted vaccine. *Vaccine* **19**, 2673–2680 (2001).

64. Grunwald, T. & Ulbert, S. Improvement of DNA vaccination by adjuvants and sophisticated delivery devices: vaccine-platforms for the battle against infectious diseases. *Clin. Exp. Vaccine Res.* **4**, 1 (2015).

65. Kutzler, M. A. & Weiner, D. B. DNA vaccines: ready for prime time? doi:10.1038/nrg2432

66. Pardi, N., Hogan, M. J. & Weissman, D. Recent advances in mRNA vaccine technology. *Curr. Opin. Immunol.* **65**, 14–20 (2020).

67. Janitzek, C. M. *et al.* Bacterial superglue generates a full-length circumsporozoite protein virus-like particle vaccine capable of inducing high and durable antibody responses. *Malar. J.* **15**, 1–9 (2016).

68. Hoffmann, M. *et al.* SARS-CoV-2 Cell Entry Depends on ACE2 and TMPRSS2 and Is Blocked by a Clinically Proven Protease Inhibitor. *Cell* **181**, 271-280.e8 (2020).

69. Reed, L.J.; Muench, H. A simple method of estimating fifty percent endpoints. *Am. J. Hugiene* **27**, 493–497 (1938).

70. Hierholzer, J. C. ; R. A. K. Virology Method Manual. in *Virology Method Manual* 374 (1996).

Acknowledgement

The authors would like to express their deep gratitude to Nahla Chehabi, Andreas Frederiksen, Benjamin Jacobsen, Elham Marjan Mohammad Alijazaeri, Ana Maria Guzunov and Tenna Gribfeldt Jensen for their excellent technical assistance. Furthermore, we would like to thank Blanca Lopez Mendez at the Biophysics Facility—Protein Structure and Function Program from Center for Protein Research, Copenhagen, for her assistance with the DLS measurement and analysis as well as the Core Facility for Integrated Microscopy, Faculty of Health and Medical Sciences, University of Copenhagen for their excellent facilities and support in acquiring TEM images. The authors would like to thank the IT, Substrate, Logistics and Security Departments at the Faculty of Health and Medical Sciences, University of Copenhagen for ensuring that this important work in the laboratory could continue during times of total lockdown. Novo Nordisk and Merck Millipore are thanked for their continuous and direct support of process development. Attana A/S, BioradChemometec, Eppendorf, Hamilton, Thermo Fisher scientific and Wyatt are thanked for their swift and direct support of the project. The preclinical development presented in this article was funded through grants from Carlsberg Foundation (Sapere Aude grant), Gudbjørg og Ejnar Honorés Fond, Independent Research Fund Denmark (No 0214-00001B (SRP)), a private donation from Line and Mads Brandt Pedersen, and the European Union's Horizon 2020 research and innovation program (No 101003608).

Author contributions:

All authors contributed to: analyzing and discussing the data and proof-reading the manuscript.

CF and LG: writing of the article, CLP, antigen and vaccine design, purification and quality control of the vaccine, mouse studies (ELISA, immunization), planning and designing CLP related experiments.

All authors from Aarhus University (MI, SRP and LSR): designed, performed and analyzed neutralization data.

All authors from Expres^{2}ion Biotechnologies (VS, MS, JD, SC, BH, TD, BWN, AS, MS, LFA): design, production, purification and characterization of protein constructs.

All authors from Leiden University (SKM, TJD, MK): designed, performed and analyzed neutralization data.

RD and EWH: designing, performing and analyzing ACE2 binding studies.

CMJ: designing and performing electron microscopy, DLS measurements, CLP production and purification, CLP, antigen and vaccine design.

KlA: performing ELISA, CLP production and purification, CLP, antigen and vaccine design.

SME, TG, SC and EVC: Large scale development of the VLPs, QC analytical method development for the VLPs.

LF: CLP production and purification, CLP, antigen and vaccine design.

ST: contributed to the design of the tag/catcher system, CLP and vaccine design.

PK and TMH: production, purification and quality control of monoclonal antibodies used for ELISA studies.

MT, SS and AGS: antigen design, production and purification.

All authors from Wageningen (LVO, GP): antigen design, production and purification.

BM (Tübingen): application for funding, providing clinical expertise.

LHH, HU, KI: provided human serum samples and analysis of it.

WAJ: creating the COVID consortium, application for funding, design of experiments, supervision of the project.

TGT, MAN, AS: application for funding, design of experiments, supervision of the project

AFS: supervising the project and writing the article, application for funding, design of experiments.

Competing interest:

CMJ, ST, TGT, AS, MAN and AFS are listed as co-inventors on a patent application covering the AP205 CLP vaccine platform technology (WO2016112921 A1) licensed to AdaptVac. Employees of AdaptVac (CF, LG, AFS, WAJ), a company commercializing virus-like particle display technology and vaccine, including several patents. ExpreS^2ion employees, as ExpreS^2ion is a listed company with IP on ExpreS^2 cells. WDJ is co-founder and owns ExpreS^2ion shares. The other authors have no financial conflicts of interest.

Figures

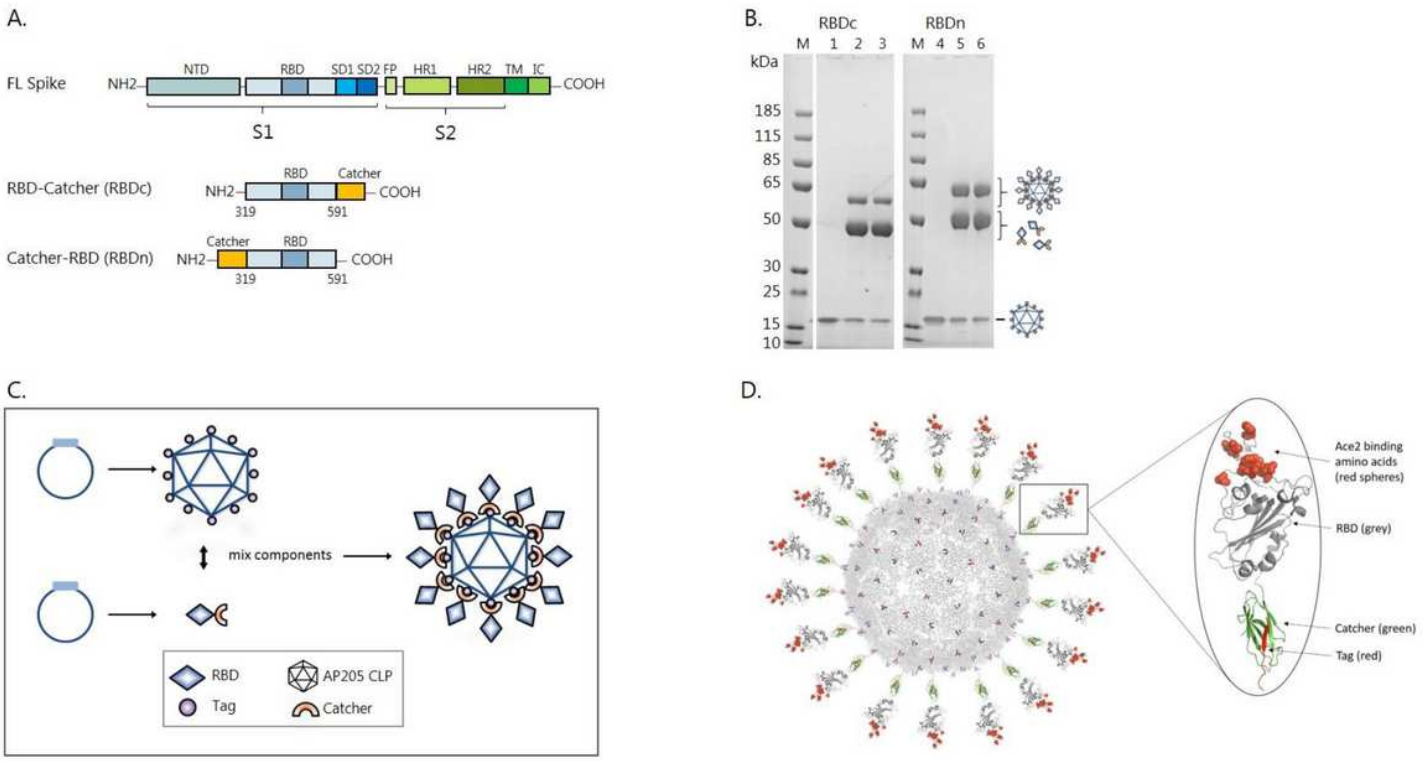

Figure 1

RBD-CLP vaccine design and characterization. (A) Schematic representation of the complete SARS-CoV-2 spike protein including the two RBD-Catcher antigen designs. NTD = N-terminal domain, FL= full-length, RBD = receptor-binding domain, SD1 =subdomain 1, SD2 = subdomain 2, FP = fusion peptide, HR1 = heptad repeat 1, HR2 = heptad repeat 2, TM = transmembrane region, IC = intracellular domain (B) Individual vaccine components on a reduced SDS-PAGE. M= marker, lane 1: unconjugated Tag-CLPs (16.5kDa), lane 2: RBDc-CLP conjugation after overnight incubation at 4°C (60kDa), lane 3: RBDc-CLP conjugation after overnight incubation at 4°C (60kDa) + spin test, lane 4: unconjugated Tag-CLPs (16.5kDa), lane 5: RBDn-CLP conjugation after overnight incubation at RT (60kDa), lane 6: RBDn-CLP conjugation after overnight incubation at RT (60kDa) + spin test. (C) Schematic representation of the Tag/Catcher-AP205 technology used to create the RBD-CLP vaccines. The genetically fused peptide Tag at the N-terminus of each AP205 capsid protein (total of 180 subunits per CLP) allows unidirectional and high-density coupling of the RBD antigen, via interaction with the N- or C-terminal Catcher (i.e. the corresponding binding partner) (D) Structural illustration of the RBD-CLP vaccine, based on the SARS-CoV-2 spike (Sequence ID: QIA20044.1), Tag/Catcher (not published), and AP205 CLP (Sequence ID: NP_085472.1)45 structures. The Tag is shown in red, Catcher in green, RBD in grey with the amino acids residues involved in ACE2 binding interface shown as red spheres.

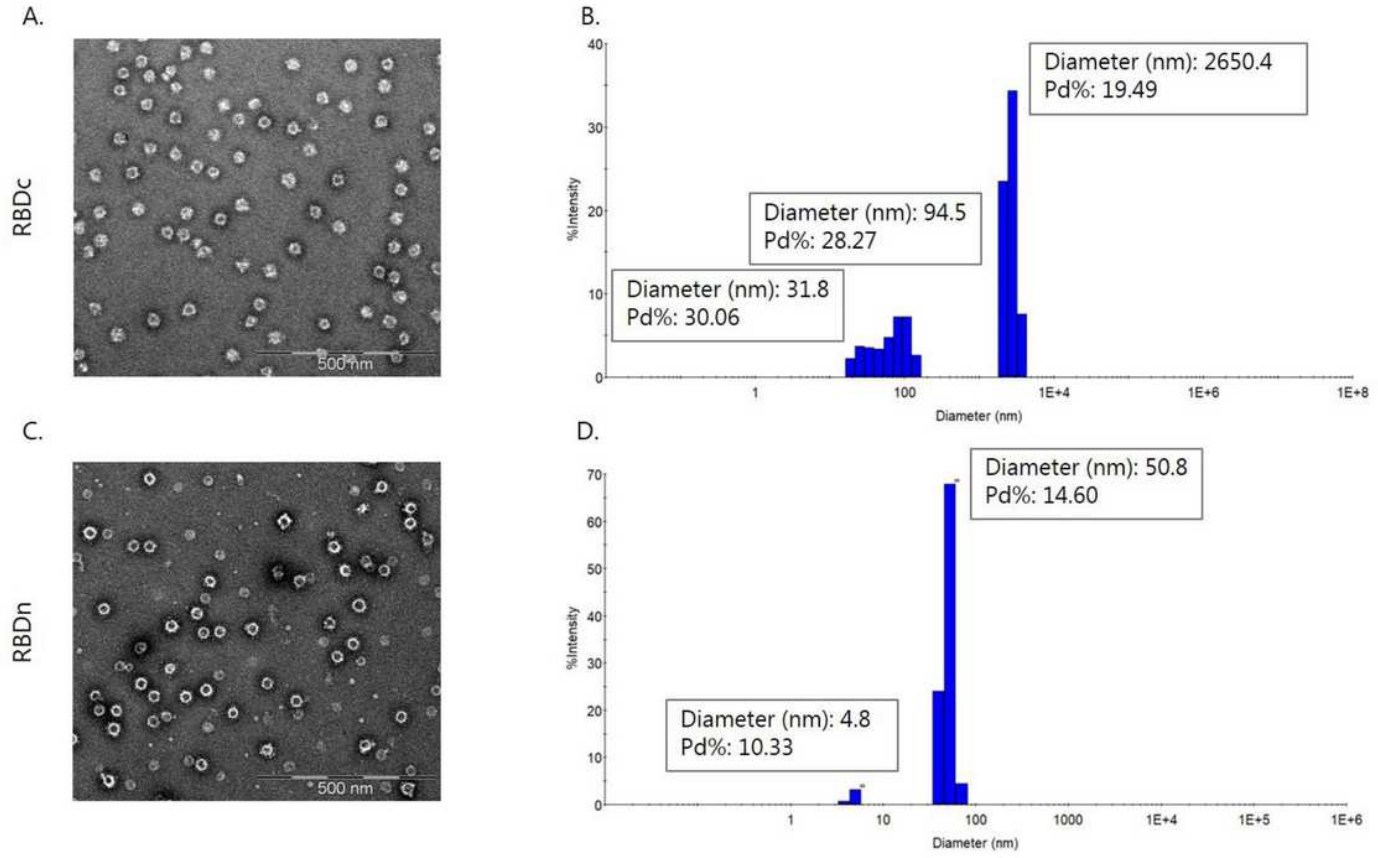

Figure 2

Vaccine quality assessment. (A,C) Transmission electron microscope (TEM) images of the negatively stained purified RBDc-CLP or RBDn-CLP vaccine. Scale bar is 500nm. (B,D) Histogram of the % intensity of the purified RBDc-CLP or RBDn-CLP particles from DLS analysis. Annotated are the average diameter and polydispersity (Pd%) for the particles.

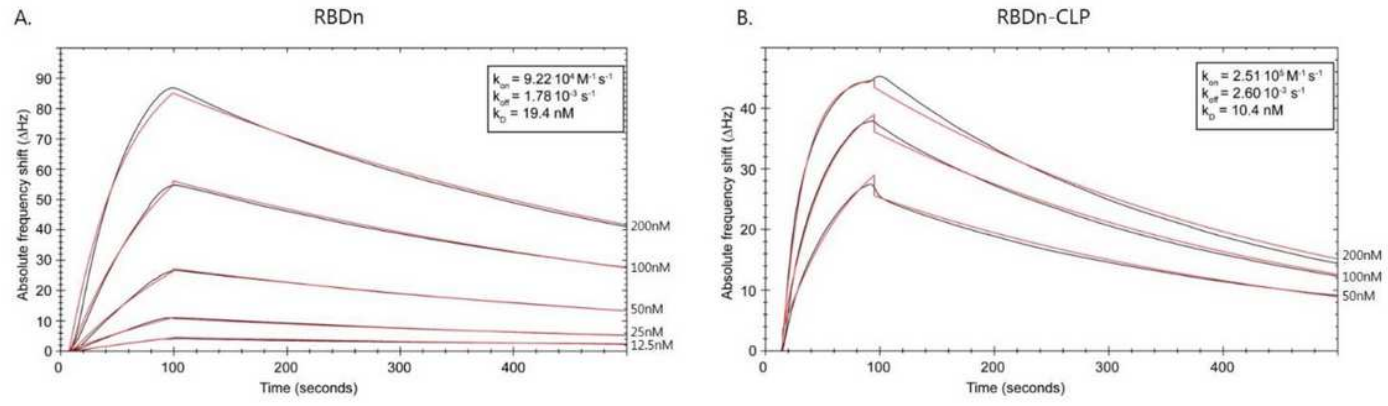

Figure 3

ACE2 binding kinetics for RBDn and RBDn-CLP (A) Real time binding (black curves) of RBDn to immobilized hACE2 on the chip surface. Red curves show theoretical curves obtained using a 1:1 simple binding model. Analyte concentrations are shown to the right and kon, koff and kD are boxed. (B) Real time binding (black curves) of ExpreS2 produced ACE2 to immobilized RBDn-CLP on the chip surface. Red curves show theoretical curves obtained using a 1:1 simple binding model. Analyte concentrations are shown to the right and kon, koff and kD are boxed.

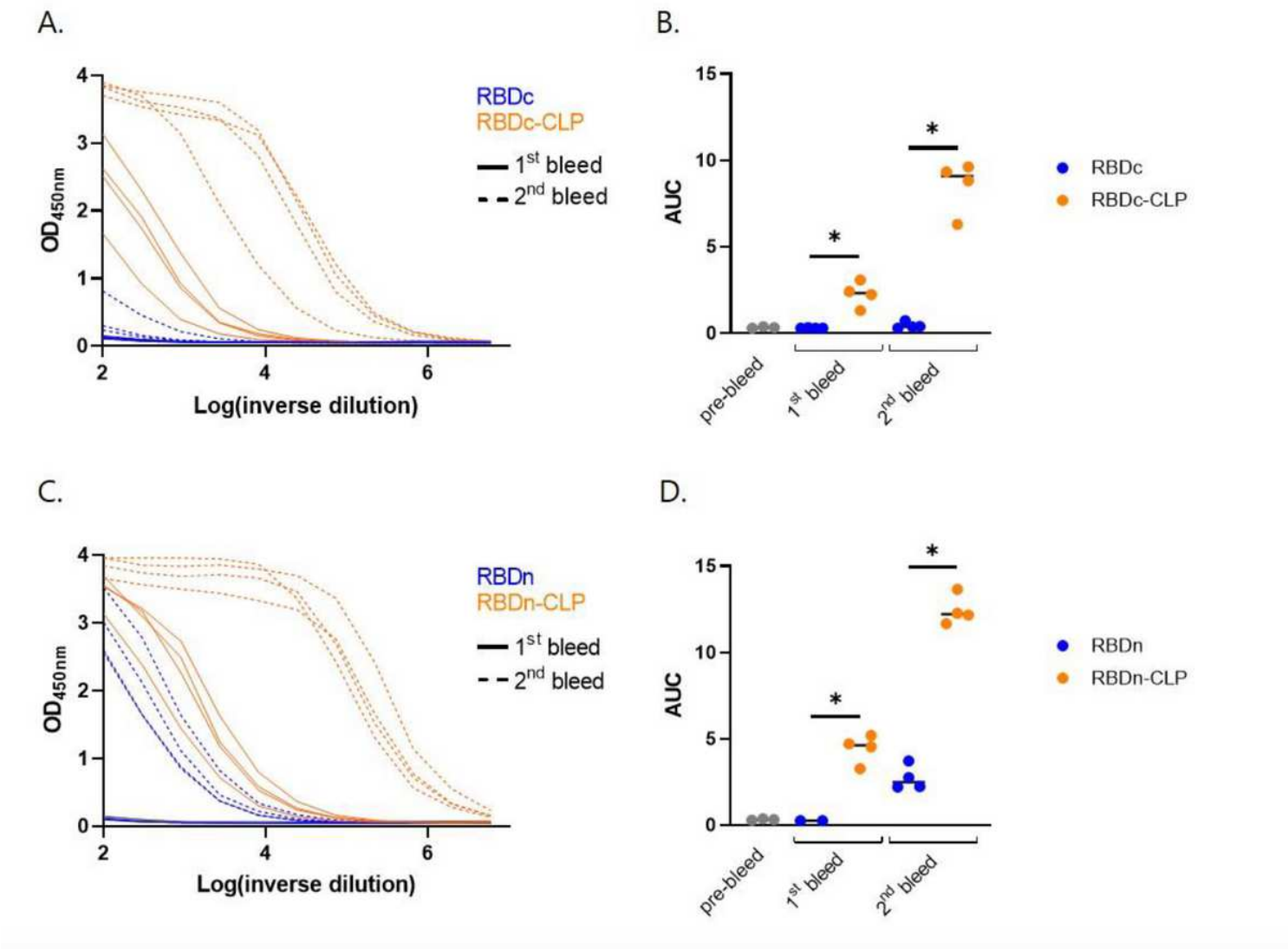

Figure 4

RBD-CLP vaccines induce high antigen-specific antibody titers in mice. (A) Dilution curves from ELISA of total anti-SARS-CoV-2 spike (aa35-1227) IgG antibodies detected in sera from BALB/c mice (n=4) immunized intramuscularly with soluble RBDc (prime 2µg / boost 2µg) or CLP-displayed RBDc (RBDc-CLP) (prime 1µg / boost 1µg). Analyzed sera was obtained before vaccination (pre-bleed), two weeks after the prime (1st bleed) or boost (2nd bleed) vaccinations. (B) ELISA results depicted in the form of area under curve (AUC), the bars represent the median. Non-parametric Mann-Whitney test was used for statistical comparison. A statistically significant ($p < 0.05$) differences are marked by the *. (C) Dilution

curves from ELISA of total anti-SARS-CoV-2 spike (aa35-1227) IgG antibodies detected in sera from Balb/c mice (n=4) immunized intramuscularly with soluble RBDn-Catcher (prime 5µg / boost 5µg) or CLP-displayed RBDn (RBDn-CLP) (prime 6.5µg / boost <0.1µg / boost 6.5µg). Analyzed sera was obtained before vaccination (pre-bleed), two weeks after the prime (1st bleeds) or after boost-boost (2nd bleed) vaccinations. (D) ELISA results depicted in the form of AUC, the bars represent the median. Non-parametric Mann-Whitney test was used for statistical comparison. A statistically significant ($p < 0.05$) differences are marked by the *.

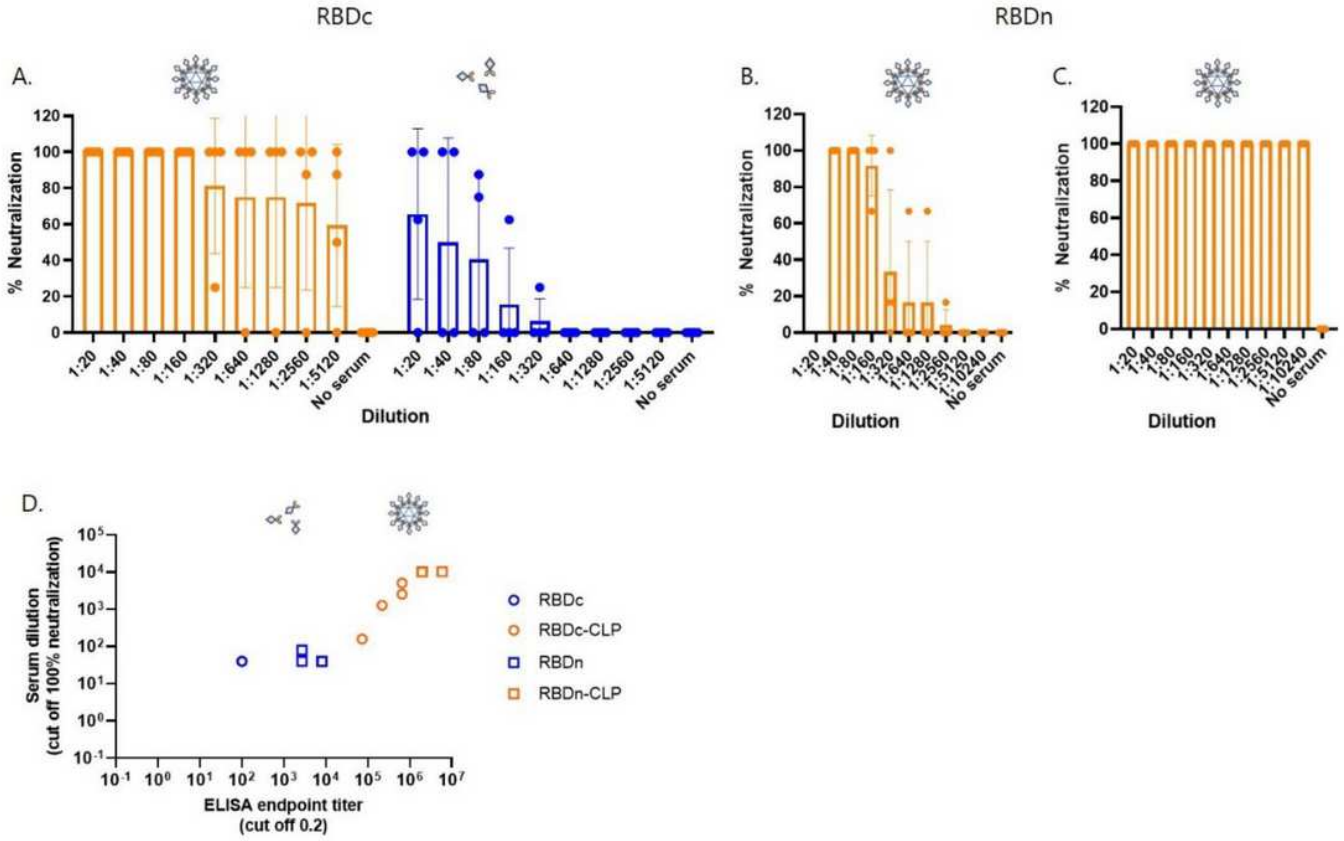

Figure 5

Serum from mice immunized with RBD-CLP vaccines neutralize SARS-CoV-2 in vitro. (A) Serum from mice immunized and boosted with RBDc-CLP (orange) (prime 1µg / boost 1µg) or soluble RBDc (blue) (prime 2µg / boost 2µg) was mixed with a SARS-CoV-2 virus and tested for cell entry. Each dot represents the percentage neutralization per mouse per dilution. Bars represent the mean and SD. (B, C) Serum from mice immunized with RBDn-CLP (prime 6.5µg / boost <0.1µg / boost 6.5µg) from first bleed after the first immunization (B) or second bleed after the booster immunizations (C), was mixed with a SARS-CoV-2 virus and tested for cell entry. Each dot represents the percentage neutralization per mouse per dilution. Bars represent the mean and SD. (D) Correlation between IgG endpoint titer (2nd bleed, cutoff 0.2) and serum dilution required for 100% virus neutralization. Endpoint titers were determined from dilution curves, by ELISA, from sera of mice immunized with RBDc (prime 2µg / boost 2µg), RBDc-CLP (prime 1µg / boost 1µg), RBDn (prime 5µg / boost 5µg) or RBDn-CLP (prime 6.5µg / boost <0.1µg / boost 6.5µg) and

correlated to the serum dilution required for 100% virus neutralization in the neutralization assay done on the same sera. Each dot represents one mouse. Pearson r Non- test was used to assess correlation.

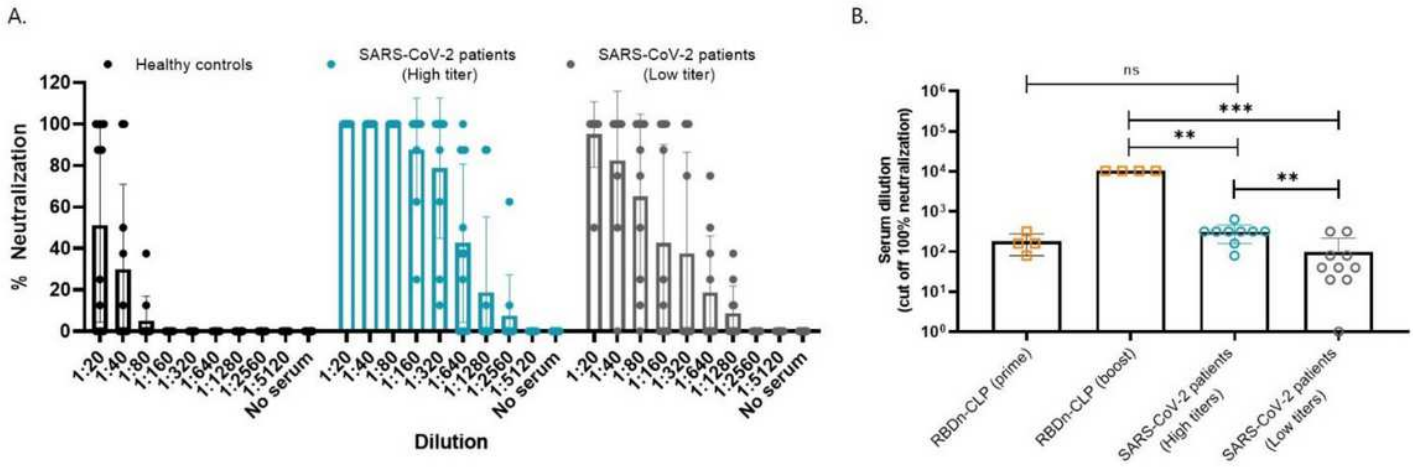

Figure 6

Neutralization capacity of serum from convalescent SARS-CoV-2 patients. (A) A dilution series of individual human plasma samples from SARS-CoV-2 patients (with either 'high' or 'low' ELISA binding titer against SARS-CoV-2 spike protein) or healthy controls were mixed with a clinical SARS-CoV-2 isolate and tested for cell entry. Each dot represents the percentage neutralization per sample, per dilution. Bars represent the mean of the group with a standard deviation. (B) Endpoint serum dilution required for 100% virus neutralization. Each dot represents the serum dilution needed for 100% virus neutralization according to the dilution titration of the sera in the neutralization assay (Fig. 6A and Fig. 5B,C). Bars represent the mean of the group with a standard deviation. Mann-Whitney test was used for statistical comparison. Statistically significant differences are marked by asterisk: ns=non-significant, **: p≤0.005, ***: p≤0,001.